

Photoinduced rotamerization and dissociation of *o*-fluorobenzoyl chloride in solid Ar

Nobuaki Tanaka*, Kohei Nakamura, Masatoshi Yutaka, Hiromasa Nishikiori
Department of Environmental Science and Technology, Faculty of Engineering, Shinshu University, 4-17-1 Wakasato, Nagano 380-8553, Japan

* Corresponding author. Fax: +81 26 269 5550.

E-mail address: ntanaka@shinshu-u.ac.jp (N. Tanaka).

ABSTRACT

UV light-induced reactions of *o*-fluorobenzoyl chloride (FBC) were investigated using infrared spectroscopy in a cryogenic Ar matrix. Photoinduced rotational isomerization from *anti*- to *gauche*-FBC was confirmed by comparison with calculated spectra. In addition, photolysis products were found to be ketene species (6-chloro-2-fluoro-2,4-cyclohexadien-1-ylidenemethanone), *o*-fluorobenzoyl radical, *o*-chlorofluorobenzene, *m*-chlorofluorobenzene and CO.

Keywords: *o*-fluorobenzoyl chloride; Ar matrix; rotational isomerization; photolysis; ketene

1. Introduction

Benzoyl chloride derivatives have been used as a reagent for the syntheses of anticancer [1], antileukemic [2] and antiadenoviral [3] agents. Despite its practical use, the available properties on the structure and spectroscopy are relatively scarce. Using gas electron diffraction, the conformations of *ortho*-halobenzoyl chloride were studied by Johansen et al. [4] who determined that as the size of a halogen atom increases, the equilibrium torsion angles of $\varphi(\text{C}(\text{X})-\text{C}-\text{C}(=\text{O})-\text{Cl})$ for *gauche* and *anti* conformers also increase due to the steric effect. They found $\varphi(\text{C}(\text{F})-\text{C}-\text{C}(=\text{O})-\text{Cl})$ to be $+44.4(24)^\circ$ and $-179.9(6)^\circ$ for *gauche*- and *anti*-*o*-fluorobenzoyl chloride (FBC), respectively, and the $\Delta G^\circ(\text{gauche}-\text{anti})$ to be $+0.48(42)$ kcal mol⁻¹ at 386 K [4]. They also performed theoretical calculations at different levels. Contrary to observations, non-planar geometries were found for both conformers, and $\varphi(\text{C}(\text{F})-\text{C}-\text{C}(=\text{O})-\text{Cl})$ was calculated to be $33.4-44.2^\circ$ and $-147.4-157.5^\circ$ for the *gauche*- and *anti*-FBCs, respectively. Despite previous investigations of the infrared spectrum of FBC [5], no spectral interpretation of conformers has been conducted.

In the photolysis of benzoyl chloride in solid Ar, a ketene species

(6-chloro-2,4-cyclohexadien-1-ylidenemethanone) was formed as an intermediate product followed by its dissociation to yield chlorobenzene and CO [6]. In contrast to the photolysis of benzaldehyde [7], the formation of a benzoyl radical was not confirmed.

In the present study, FBC's infrared spectra were measured in a low-temperature Ar matrix. Due to the narrower bandwidth and lesser complexity of the spectrum in the matrix-isolated species than in vapour and liquid, the absorption bands for different conformers can be separated. Coexistence of the *anti* and *gauche* conformers was confirmed in FBC through matrix-isolation infrared spectroscopy combined with UV irradiation and DFT calculations. The observed infrared bands of each conformer were separated and assigned.

2. Experimental

FBC (Wako Pure Chemicals Industries, Ltd.) was purified by a freeze–pump–thaw cycle at 77 K and was diluted with argon gas (Nippon Sanso, Japan, 99.999 % purity) to approximately 1/1000 (0.2 Torr FBC and 200 Torr Ar). It was then slowly sprayed onto a CsI plate cooled by a closed-cycle helium refrigerator (Iwatani CryoMini M310/CW303) to approximately 7 K. For product identification, *o*- and *m*-chlorofluorobenzenes (CFB, Wako Pure Chemicals Industries, Ltd.) were used as authentic samples. Infrared absorption spectra were measured in the 4000–700 cm^{-1} range with a resolution of 1.0 cm^{-1} using a SHIMADZU FTIR 8300 spectrophotometer equipped with a liquid-nitrogen-cooled MCT detector. Each spectrum was obtained by acquiring 128 scans. Under the sample conditions mentioned above, the populations of conformers just after deposition were assumed to be the same as those at the temperature of the gaseous sample just before deposition (298 K). The photoexcitation effect was examined by irradiating the deposited samples with UV light for 1–300 min. A Xe short arc lamp (HAMAMATSU, C2577) with a bandpass filter (HOYA, U340, $260 < \lambda < 380$ nm) or a low-pressure mercury short arc lamp (HAMAMATSU L937-04, $\lambda > 253.7$ nm) was used as the UV light source combined with a water filter to avoid thermal radiation. The UV–Vis absorption spectrum was measured with a SHIMADZU UV-3150 spectrophotometer.

For product identification and energetic consideration, a molecular orbital calculation was performed using the GAUSSIAN 09 program [8]. Geometry optimizations were performed using the Becke's three-parameter hybrid density functional in combination with the Lee–Yang–Parr correlation functional (B3LYP) and the 6-311++G(3df,3pd) basis set [9, 10]. A harmonic vibrational frequency calculation

was performed to confirm the predicted structures as local minima or transition state and to elucidate the zero-point vibrational energy corrections. The vertical transition energies of the parent and intermediate species were calculated at the TD B3LYP/6-311++G(3df,3pd) level and at the SAC-CI/D95+(d,p) level based on the structures optimized at the CCSD/D95+(d,p) level.

3. Results and discussion

3.1 Separation and assignments of the infrared bands of the conformers

An FBC/Ar mixture was deposited on a CsI window (FBC/Ar = 1/1000). In the infrared spectrum obtained after deposition, strong bands were observed at 1794 and 886 cm^{-1} , which were attributed to the C=O and C–Cl stretching vibrations of FBC, respectively [5]. Fig. 1 shows (a) the observed infrared difference spectrum obtained by subtracting the spectrum measured before Hg lamp irradiation from that measured after 120 min of irradiation and (b) the calculated infrared difference spectra of FBC, where the upward and downward bands of the calculated spectra correspond to those of the *gauche* and *anti* conformers, respectively. The irradiation resulted in a decrease and an increase in intensities of the bands due to a reactant with the appearance of new bands. Among the reactant bands, the bands at 1748, 1716, 1624, 1490, 1456, 1276, 1230, 1203, 1140, 1108, 899, 895, 823, 772 and 745 cm^{-1} showed growth and decay behaviour during the irradiation period. FBC exhibits UV absorption in the 260–300 nm region based on the $S_2(\pi, \pi^*) \leftarrow S_0$ transitions shown in Fig. S1. The calculated spectra at the B3LYP/6-311++G(2d,2p) level with anharmonic treatment reproduced well the observed spectrum. Comparison of the observed and calculated spectra indicates that the bands that decreased and increased upon UV irradiation correspond to those of the *anti* and *gauche* conformers, respectively. The calculation at the B3LYP/6-311++G(3df,3pd) level shows that the *anti* conformer is more stable than the *gauche* conformer by $4.9 \times 10^2 \text{ cm}^{-1}$ (1.4 kcal mol^{-1}). This indicates that the *gauche/anti* population ratio before UV irradiation is 0.096/1 at 298 K. The barrier height for the conversion from the *anti* to the *gauche* conformer was calculated to be $9.8 \times 10^2 \text{ cm}^{-1}$ (2.8 kcal mol^{-1}) in the ground state, indicating that the conversion between the *anti* and *gauche* conformers is not expected to occur at 7 K in the absence of UV irradiation. UV irradiation yielded an increase in the population of the less stable conformer. The observed and calculated wavenumbers of the infrared bands in the 2000–700 cm^{-1} region are given in Table 1.

3.2 Identification of other products

At a wavelength of 253.7 nm from an Hg lamp, the absorption of FBC was relatively weak. Therefore, we performed a broadband irradiation from a filtered Xe lamp. The UV irradiation using the Xe lamp promoted the reaction to clearly discern growth bands in the difference spectra in addition to the vibration bands of the *gauche*-FBC. The bands that increased in intensity were classified into two groups (A and B) by their different initial formation rates. The evolutions of the integrated absorbance at 752 cm⁻¹ for group A and at 2142 cm⁻¹ for group B over time are shown in Fig. 2. To clarify the growth behaviours, each curve was normalized by the value measured at the 300 min irradiation time. The absorption bands from groups A and B continued to grow during the irradiation period. However, group A's absorption band would continue to grow, while group B's nearly reached a maximum at the 300 min irradiation time. Fig. 3 shows the difference spectrum obtained by subtracting the spectrum measured after UV irradiation for 240 min from that measured after UV irradiation for 300 min. The wavenumbers of group A agree with those of authentic *o*- and *m*-CFBs measured in Ar. The bands at 1593, 1488, 1452, 1288, 1266, 1237, 1128, 1072, 1030, 828 and 752 cm⁻¹ were attributed to C–C stretching, C–H in-plane bending, C–H in-plane bending, C–H in-plane bending, C–C stretching, C–F stretching, C–H in-plane bending, CCC in-plane bending, C–C stretching, CCC in-plane bending and C–H out-of-plane bending vibrations of *o*-CFB, respectively [11-13]. The band at 1245 cm⁻¹ may be due to the overtone or the combination band. The bands at 1228, 1083, 1063, 860 and 776 cm⁻¹ were attributed to C–F stretching, C–H in-plane bending, C–H in-plane bending, C–H out-of-plane bending and C–H out-of-plane bending vibrations of *m*-CFB, respectively [11, 12]. The infrared absorption band intensities for *o*-CFB (752 cm⁻¹) and *m*-CFB (776 cm⁻¹) calculated at the B3LYP/6-311++G(3df,3pd) level were used to calculate the product yield ratio, $\phi_{o\text{-CFB}}/\phi_{m\text{-CFB}}$, and the ratio was found to be 8.8 at the 300 min irradiation time. The formation of *o*-CFB was found to be the major reaction path in the Ar matrix in the present condition. The bands at 805 and 736 cm⁻¹ were tentatively assigned to C–F stretching and C–H out-of-plane bending vibrations of the 2-fluorophenyl radical, respectively.

Fig. 4 shows the difference spectrum obtained by subtracting the spectrum measured before UV irradiation from that measured after UV irradiation for 60 min. Two strong bands were observed at 2142 and 2139 cm⁻¹. The latter band behaved as a group A band after prolonged irradiation. Ketene species and CO absorption bands are known to emerge in the ~2140 cm⁻¹ region [14-16]. In fact, in the photolysis of benzoyl chloride the ketene product showed the absorption band assigned to the C=C=O asymmetric stretching vibration at 2120 cm⁻¹ and the CO product showed the

absorption band at 2138 cm^{-1} [6]. The CO was produced almost concomitantly with the formation of chlorobenzene from the intermediate ketene species. Therefore, the band at 2139 cm^{-1} was assigned to the vibration band of CO whose wavenumber was slightly blue-shifted due to the presence of the adjacent band. Ketene species might be produced in the photolysis of FBC. Fig. S2 shows the calculated spectra of the two possible ketene species, 6-chloro-2-fluoro-2,4-cyclohexadien-1-ylidenemethanone (CHM) and 6-chloro-6-fluoro-2,4-cyclohexadien-1-ylidenemethanone (CHM2), arising from the *anti*- and *gauche*-FBCs, respectively, and a ketene radical (CHMR) calculated at the B3LYP/6-311++G(2d,2p) level with anharmonic treatment. The molecular structures are shown in Fig. S3. The CHMR can be excluded from the candidates due to the lower wavenumber of 2011 cm^{-1} for the C=C=O asymmetric stretching vibration. The intensities of the bands at 1162 cm^{-1} for CHM and 1022 cm^{-1} for CHM2 are comparable to those of the bands at 833 and 842 cm^{-1} , respectively. In Fig. 4, a relatively strong band is present at 1175 cm^{-1} , whereas in the $1050\text{--}1000\text{ cm}^{-1}$ region only weak bands are present. The observed spectrum was well reproduced by the calculated spectrum for the CHM from *anti*-FBC. The yield of CHM2 from *gauche*-FBC is low due to the initial low population of *gauche*-FBC compared with that of *anti*-FBC. Among the group B bands not attributed to CHM, the band at 1847 cm^{-1} suggests the formation of a carbonyl compound. Judging from the growth behavior, the band at 1847 cm^{-1} is due to one of primary products. The C–Cl bond dissociated product, *o*-fluorobenzoyl radical (FBR), will be a candidate. The calculation showed the existence of *anti*- and *syn*-FBRs due to the difference in the direction of the C=O bond as to the fluorine atom. The *anti*-FBR was calculated to be 0.3 kcal mol^{-1} more stable than *syn*-FBR. The observed wavenumber of 1847 cm^{-1} was blue-shifted by 22.6 cm^{-1} from that of C=O stretching vibration band of benzoyl radical in Ar [17]. The anharmonic wavenumbers of the C=O stretching vibration of *anti*- and *syn*-FBRs were calculated to be 1843 and 1858 cm^{-1} , respectively, which were shifted by -4 and $+11\text{ cm}^{-1}$ from the calculated value of 1847 cm^{-1} for benzoyl radical, respectively. Comparison in the trend suggests the formation of *syn*-FBR. Though the *anti*-FBR was calculated to be more stable than *syn*-FBR, conformation of the fluoro and carbonyl groups was preserved during the photolysis. Hence, species attributed to group B bands were identified with CHM and tentatively *syn*-FBR. Table 2 lists the observed and calculated wavenumbers of the intermediate products.

3.3. Reaction mechanism

Along with the absorption band caused by CO, the bands caused by *o*-CFB continued to increase with time and became the main bands seen in Fig. 4. The proposed reaction mechanism for the photolysis of FBC is shown in Scheme 1. The optimized structures of the intermediates and transition states are shown in Fig. S2. Fig. 5 shows the energy diagram for FBC photolysis calculated at the (U)B3LYP/6-311++G(3df,3pd) level. The vertical transition energies for *anti*- and *gauche*-FBCs were calculated at the SAC-CI/D95+(d,p)//CCSD/D95+(d,p) level. The S₁ (4.11 eV), S₂ (4.25 eV) and S₃ (5.23 eV) states of *anti*-FBC were characterized as the nπ* (HOMO-2 → LUMO), ππ* (HOMO → LUMO) and ππ* (HOMO-1 → LUMO) states with oscillator strengths of 0.006, 0.025 and 0.205, respectively. The photon energy at a wavelength of 260 nm corresponds to 110 kcal mol⁻¹ (4.77 eV), and this energy will excite FBC into the S₂ state as shown in Fig. S1. In the Franck-Condon region, two triplet states, T₁ (3.51 eV, ππ*) and T₂ (4.00 eV, nπ*), were calculated to exist below the S₁ state. The carbonyl compounds are known to undergo α dissociation in the singlet and triplet nπ* states. Hence, FBC will photodissociate to form an *o*-fluorobenzoyl radical and a chlorine atom. Since both the S₁ and T₂ states are characterized as nπ* states, the intersystem crossing from the S₁ to T₂ state would not be efficient due to the El-Sayed rule [18]. Therefore, the reaction will prefer to proceed in the singlet state. With respect to the geometry of the PhCO group, distinctly different *o*-fluorobenzoyl radical structures, a linear and a bent form, exist, which were given the name CHMR and FBR in §3.2, respectively. The formation of CHMR is symmetry-allowed because of the correlation between the states [19]. The energy difference between CHMR and *syn*-FBR was calculated to be 3.7 kcal mol⁻¹, which is relatively small compared with the energy of the acetyl radical (25 kcal mol⁻¹). This small energy difference is caused by resonance stabilization in the linear structure. Therefore, CHMR and the chlorine atom that are produced will recombine to form CHM in the matrix cage. Alternatively, a vibrationally excited S₀ state of FBC may be produced when the efficient internal conversion from the S₁ state occurs. The calculated transition state, TS2, connecting the *anti*-FBC in the S₀ state and CHM, has an energy of 42.8 kcal mol⁻¹. The imaginary frequency of TS2 was calculated to be 180i cm⁻¹ at the B3LYP/6-311++G(3df,3pd) level. The TD B3LYP calculation gave vertical transition energies of the CHM S₁, S₂, S₃ and S₄ states of 2.87, 3.73, 4.43 and 4.86 eV with oscillator strengths of 0.001, 0.123, 0.002 and 0.015, respectively. CHM can reach the S₃ state when it is irradiated at λ > 260 nm. The molecular orbital (LUMO+1) possessing a σ_{C-Cl}* character contributes to the excited states of S₁, S₂ and S₃. Once the CHM is excited upon irradiation, C-Cl bond dissociation occurs to form CHMR and Cl.

Then, the CHMR may release CO to form a 2-fluorophenyl radical (FPR) upon UV irradiation. This is analogous to the dissociation of $\text{CH}_2=\text{C}=\text{O}$ [20]. In fact, the MOs of the $\text{C}=\text{C}=\text{O}$ moiety of CHMR are relevant to those of $\text{CH}_2=\text{C}=\text{O}$. The other intermediate product, FBR, will also dissociate to form FPR and CO. Since the CHMR and FBR can reach the D_{12} and D_9 states upon UV irradiation, respectively, the dissociation paths will be complicated. Otherwise, followed by the recombination with the Cl atom in the matrix cage, *o*-CFB will be formed. When a recombination of the Cl atom was attained at C(6) of the FPR to yield carbene, the ensuing hydrogen atom migration resulted in *m*-CFB formation. The TS energy for the hydrogen atom migration was calculated to be $0.3 \text{ kcal mol}^{-1}$ at the B3LYP/6-311++G(3df,3pd) level in the singlet state which was $7.1 \text{ kcal mol}^{-1}$ lower compared with that for Cl atom migration.

4. Conclusions

UV light-induced reactions of FBC were investigated using infrared spectroscopy in a cryogenic Ar matrix. Photoinduced rotational isomerization from *anti*- to *gauche*-FBC was confirmed by comparison with calculated spectra. In addition, the photolysis products were found to be 6-chloro-2-fluoro-2,4-cyclohexadien-1-ylidenemethanone, *o*-fluorobenzoyl radical, *o*-chlorofluorobenzene, *m*-chlorofluorobenzene and CO.

Figure captions

Fig. 1. (a) IR difference spectrum upon Hg lamp irradiation of the matrix FBC/Ar = 1/1000 obtained by the spectral subtraction of 120–0 min. (b) Calculated infrared spectra of *anti*-FBC (downward) and *gauche*-FBC (upward) at the B3LYP/6-311++G(2d,2p) level with anharmonic correction.

Fig. 2. Integrated absorbance changes of the bands at 752 (■) and 2142 (○) cm^{-1} upon UV irradiation of the matrix FBC/Ar = 1/1000.

Fig. 3. IR difference spectrum upon Xe lamp irradiation of the matrix FBC/Ar = 1/1000 obtained by the spectral subtraction of 300–240 min.

Fig. 4. (a) IR difference spectrum upon Xe lamp irradiation of the matrix FBC/Ar = 1/1000 obtained by the spectral subtraction of 60–0 min.

Fig. 5. Potential energy diagram for the FBC photolysis calculated at the (U)B3LYP/6-311++G(3df,3pd) level of theory. The singlet excited state energies were the transition energies calculated at the SAC-CI/D95+(d,p) level for FBC and TD B3LYP/6-311++G(3df,3pd) level for CHM.

Fig. S1. Absorption spectrum of FBC in vapour (0.02 Torr, 10 cm path length). Bar graphs represent the calculated oscillator strengths of *anti*-FBC calculated at the SAC-CI/D95+(d,p) level.

Fig. S2. Calculated spectral patterns of (a) CHM, (b) CHM2 and (c) CHMR at the (U)B3LYP/6-311++G(2d,2p) level of theory with anharmonic correction.

Fig. S3. Optimized structures of intermediates and transition states calculated at the (U)B3LYP/6-311++G(3df,3pd) level of theory.

References

- [1] S. Cortez-Maya, E.C. Cortes, S. Hernández-Ortega, T.R. Apan, M. Martínez-García, *Synth Comm* 42 (2012) 46.
- [2] D.S. Prasanna, C.V. Kavitha, K. Vinaya, S.R. Ranganatha, S.C. Raghavan, K.S. Rangappa, *Eur J Med Chem* 45 (2010) 5331.
- [3] C.T. Öberg, M. Strand, E.K. Andersson, K. Edlund, P.N.T. Nam, Y.F. Mei, G. Wadell, M. Elofsson, *J Med Chem* 55 (2012) 3170.
- [4] T.H. Johansen, P.I. Dahl, K. Hagen, *Struct Chem* 24 (2013) 789.
- [5] H.N. Al-Jallo, M.G. Jalhoom, *Spectrochim Acta* 28A (1972) 1655.
- [6] N. Tanaka, *Int Res J Pure Appl Chem* 4 (2014) 737.
- [7] N. Kuş, A. Sharma, I. Reva, L. Lapinski, R. Fausto, *J Chem Phys* 136 (2012) 144509.
- [8] M.J. Frisch, G.W. Trucks, H.B. Schlegel, G.E. Scuseria, M.A. Robb, J.R. Cheeseman, G. Scalmani, V. Barone, B. Mennucci, G.A. Petersson, H. Nakatsuji, M. Caricato, X. Li, H.P. Hratchian, A.F. Izmaylov, J. Bloino, G. Zheng, J.L. Sonnenberg, M. Hada, M. Ehara, K. Toyota, R. Fukuda, J. Hasegawa, M. Ishida, T. Nakajima, Y. Honda, O. Kitao, H. Nakai, T. Vreven, J. Montgomery, J. A., J.E. Peralta, F. Ogliaro, M. Bearpark, J.J. Heyd, E. Brothers, K.N. Kudin, V.N. Staroverov, T. Keith, R. Kobayashi, J. Normand, K. Raghavachari, A. Rendell, J.C. Burant, S.S. Iyengar, J. Tomasi, M. Cossi, N. Rega, N.J. Millam, M. Klene, J.E. Knox, J.B. Cross, V. Bakken, C. Adamo, J. Jaramillo, R. Gomperts, R.E. Stratmann, O. Yazyev, A.J. Austin, R. Cammi, C. Pomelli, J.W. Ochterski, R.L. Martin, K. Morokuma, V.G. Zakrzewski, G.A. Voth, P. Salvador, J.J. Dannenberg, S. Dapprich, A.D. Daniels, Ö. Farkas, J.B. Foresman, J.V. Ortiz, J. Cioslowski, D.J. Fox, *Gaussian 09, Revision D.01*, Gaussian, Inc.: Wallingford, CT (2013)
- [9] A.D. Becke, *J Chem Phys* 98 (1993) 5648.
- [10] C. Lee, W. Yang, R.G. Parr, *Phys Rev B* 37 (1988) 785.
- [11] N.D. Patel, V.B. Kartha, N.A. Narasimham, *J Mol Spectrosc* 48 (1973) 185.

- [12] N.D. Patel, V.B. Kartha, N.A. Narasimham, *J Mol Spectrosc* 48 (1973) 202.
- [13] J.H.S. Green, *Spectrochim Acta* 26A (1970) 1913.
- [14] N. Tanaka, *Open J Phys Chem* 4 (2014) 117.
- [15] T. Tamezane, N. Tanaka, H. Nishikiori, T. Fujii, *Chem Phys Lett* 423 (2006) 434.
- [16] N. Tanaka, M. Nakata, *Int Res J Pure Appl Chem* 4 (2014) 762.
- [17] A. Mardyukov, W. Sander, *Eur J Org Chem* (2010) 2904.
- [18] M.A. El-Sayed, *J Chem Phys* 38 (1963) 2834.
- [19] N.J. Turro, V. Ramamurthy, J.C. Scaiano, *Modern Molecular Photochemistry of Organic Molecules*, University Science Books, Sausalito, CA, 2010.
- [20] H. Xiao, S. Maeda, K. Morokuma, *J Phys Chem A* 117 (2013) 7001.

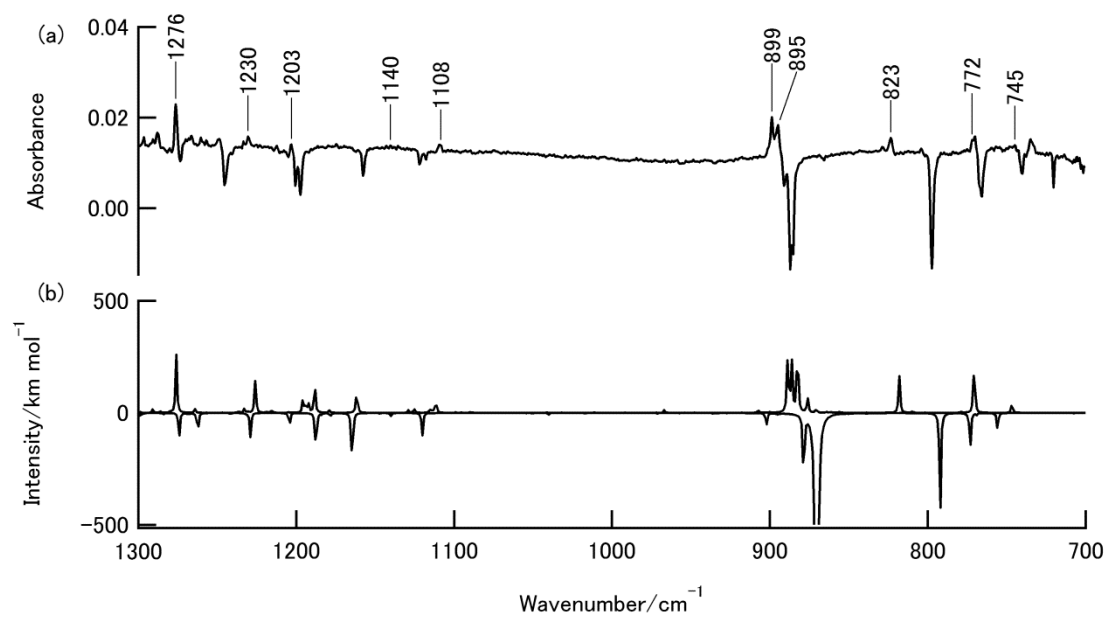


Fig. 1

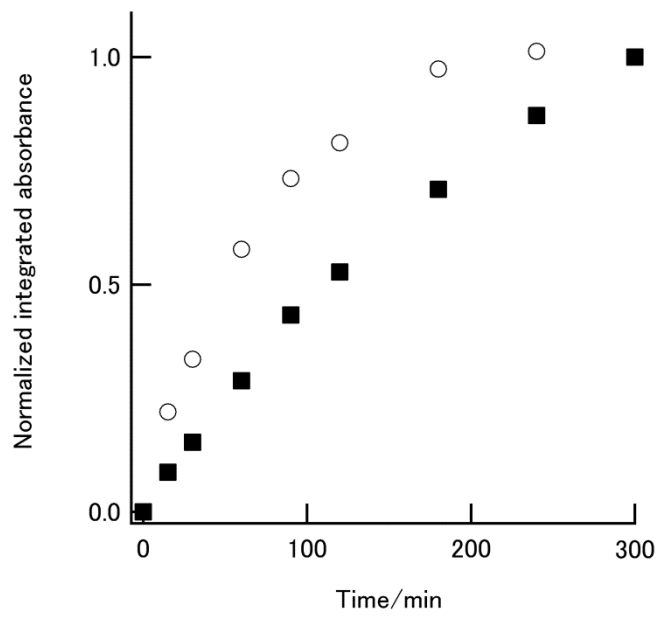


Fig. 2

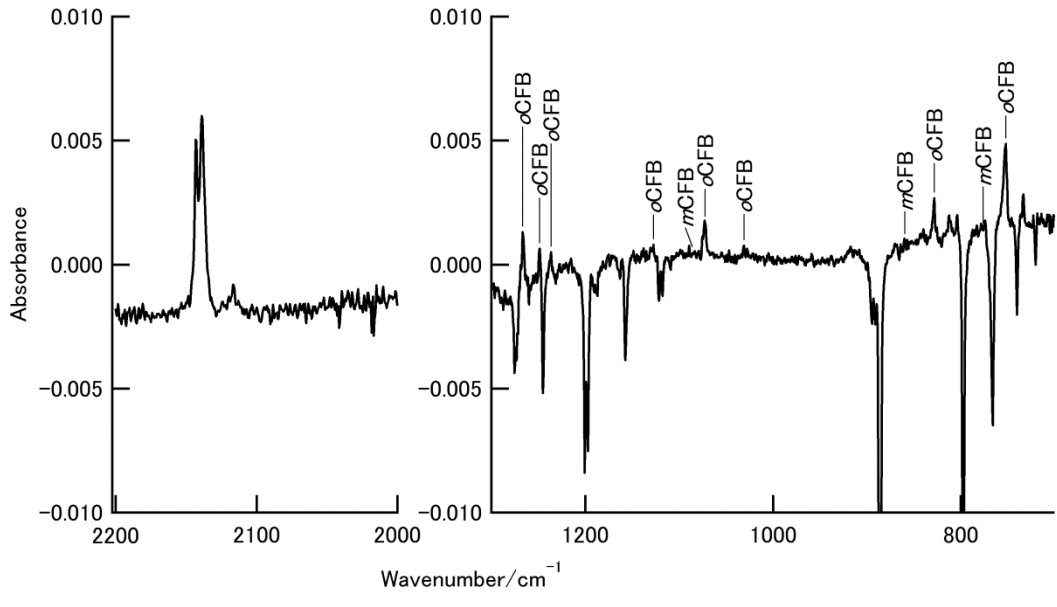


Fig. 3

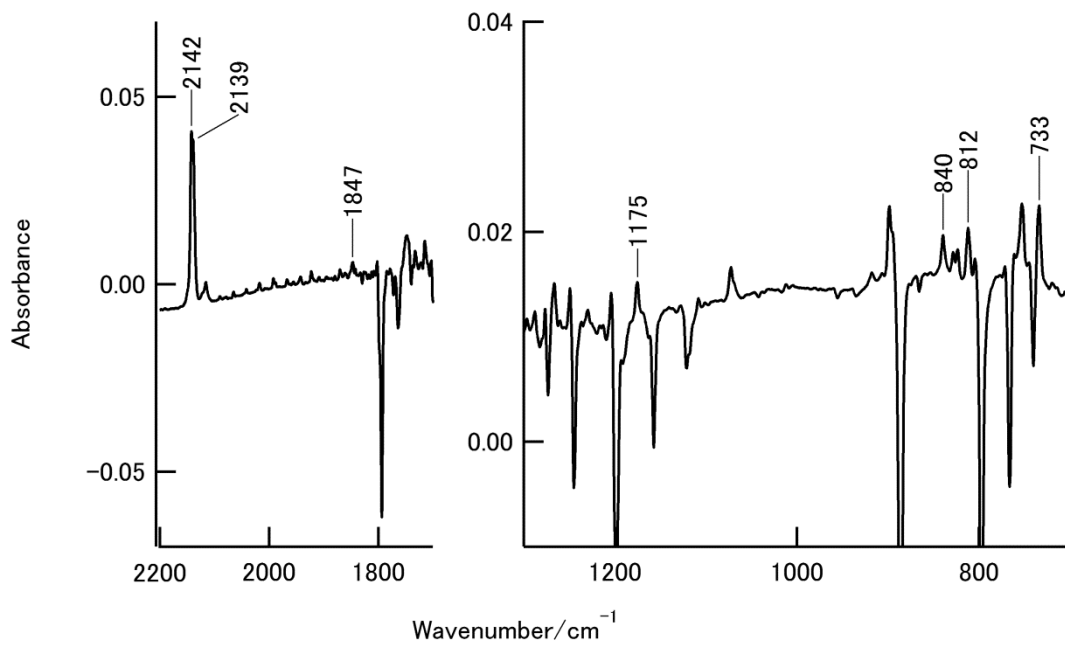


Fig. 4

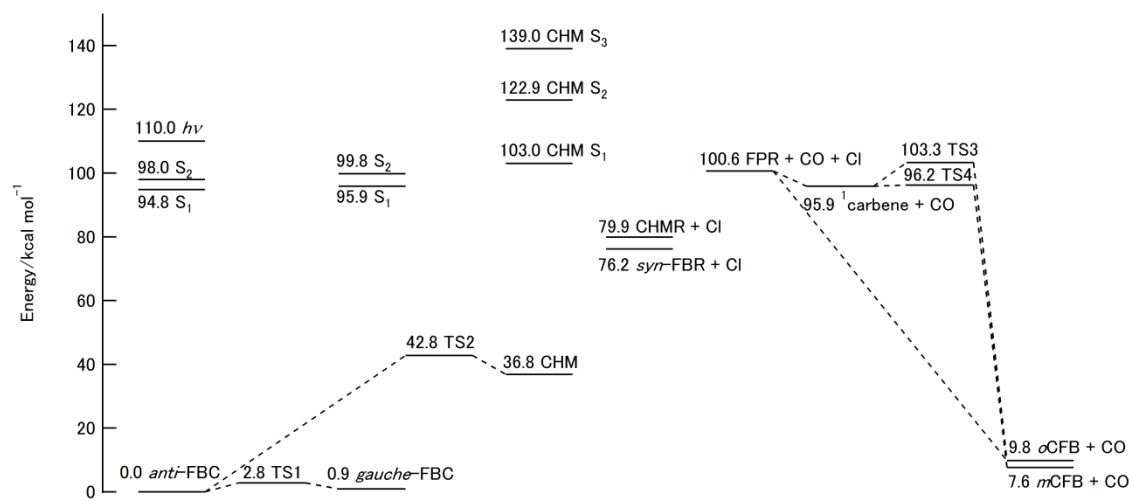


Fig. 5

Table 1

Wavenumbers (cm⁻¹), intensities and assignments of *anti*- and *gauche*-FBCs.

| species | obs | | calc ^a | | assignment |
|----------------------|-------|-------|-------------------|-------|--|
| | ν | I^b | ν | I^c | |
| <i>anti</i> - FBC | | | | | |
| | 1799 | s | 1828 | 57 | combination band of in-plane CH deform and in-plane CCl deform |
| | 1794 | vs | 1823 | 246 | CO stretch |
| | 1764 | m | 1754 | 14 | overtone band of in-plane CCC deform |
| | 1613 | s | 1601 | 42 | CC stretch |
| | 1580 | w | 1568 | 11 | CC stretch |
| | 1486 | s | 1477 | 50 | in-plane CH deform |
| | 1459 | m | 1458 | 27 | in-plane CH deform |
| | 1308 | vw | 1308 | 3 | CC stretch |
| | 1273 | m | 1274 | 29 | in-plane CH deform |
| | 1245 | m | 1229 | 53 | CF stretch |
| | 1201 | s | 1188 | 49 | CC stretch |
| | 1197 | s | 1204 | 15 | combination band of out-of-plane CH deform and out-of-plane CCC deform |
| | 1188 | w | 1178 | 4 | combination band of out-of-plane CO deform and out-of-plane CF deform |
| | 1163 | w | 1140 | 4 | combination band of in-plane CCl deform and in-plane CCC deform |
| | 1157 | m | 1165 | 68 | in-plane CH deform |
| | 1122 | w | 1120 | 28 | in-plane CH deform |
| | 1118 | w | | | |
| | 1042 | vw | 1040 | 2 | CC stretch |
| | 1031 | vw | 1017 | 0.7 | out-of-plane CH deform |
| | 955 | vw | 971 | 1 | out-of-plane CH deform |
| | 891 | m | 902 | 16 | overtone of CCl stretch |
| | 887 | vs | 879 | 84 | in-plane CCC deform + in-plane COCl deform |
| | 885 | vs | | | in-plane CCC deform + in-plane COCl deform |
| | 866 | vw | 870 | 1190 | out-of-plane CH deform |
| | 821 | vw | 839 | 1 | combination band of CCl stretch and in-plan |

| | | | | |
|----------------|----|------|-----|--|
| | | | | e CF deform |
| 798 | vs | 792 | 117 | in-plane CCC deform + in-plane COCl deform |
| 766 | s | 773 | 41 | out-of-plane CH deform |
| 740 | m | 756 | 20 | out-of-plane CCC |
| <i>gauche-</i> | | | | |
| FBC | | | | |
| 1748 | | 1800 | 110 | CO stretch |
| 1716 | | 1780 | 197 | combination band of in-plane CH deform and in-plane CCl deform |
| 1624 | | 1604 | 73 | CC stretch |
| | | 1572 | 19 | CC stretch |
| 1490 | | 1486 | 51 | in-plane CH deform |
| 1456 | | 1455 | 51 | in-plane CH deform |
| | | 1306 | 0.2 | CC stretch |
| 1276 | | 1276 | 94 | in-plane CH deform |
| 1230 | | 1226 | 44 | CF stretch |
| 1203 | | 1188 | 83 | CC stretch |
| 1140 | | 1162 | 22 | in-plane CH deform |
| 1108 | | 1112 | 25 | out-of-plane CH deform |
| | | 1042 | 0.7 | CC stretch |
| | | 1011 | 0.6 | out-of-plane CH deform |
| | | 967 | 3 | out-of-plane CH deform |
| 899 | | 889 | 73 | combination band of β CCC and β CCl |
| 895 | | 883 | 85 | in-plane COCl deform |
| | | 870 | 15 | out-of-plane CH deform |
| 823 | | 818 | 41 | in-plane CCC deform |
| 772 | | 770 | 56 | out-of-plane CH deform |
| 745 | | 747 | 11 | out-of-plane CCC deform |

^a Calculated at the B3LYP/6-311++G(2d,2p) level with the anharmonic correction.

^b Relative intensities. vs, very strong; s, strong; m, medium; w, weak; vw, very weak.

^c Intensities in km mol^{-1} .

Table 2

Wavenumbers (cm^{-1}), intensities (km mol^{-1}) and assignments of intermediate products.

| species | obs | calc ^a | | assignment |
|-----------------|-------------------|-------------------|------|----------------------------------|
| | ν | ν | I | |
| CHM | | | | |
| | 2142 | 2162 | 910 | CO stretch |
| | 1690 | 1656 | 42 | CC stretch |
| | 1544 | 1549 | 82 | CC stretch |
| | 1434 | 1426 | 32 | in-plane CH deform |
| | | 1401 | 17 | in-plane CH deform |
| | | 1319 | 17 | CC stretch |
| | | 1254 | 25 | CC stretch |
| | | 1241 | 11 | in-plane CH deform |
| | | 1176 | 7 | in-plane CH deform |
| | | 1175 | 1162 | 45 |
| | | 1120 | 11 | HCCl deform |
| | 1012 | 1027 | 5 | in-plane CH deform |
| | | 970 | 8 | CC stretch |
| | | 981 | 0 | out-of-plane CH deform |
| | | 851 | 5 | out-of-plane CH deform |
| | 812 | 833 | 47 | in-plane CCC deform + CF stretch |
| | 733 | 756 | 96 | out-of-plane CH deform |
| | | 708 | 8 | CC stretch |
| <i>syn</i> -FBR | | | | |
| | 1847 | 1858 | 253 | CO stretch |
| | 1592 | 1598 | 60 | CC stretch |
| | | 1570 | 14 | CC stretch |
| | 1474 ^b | 1469 | 35 | in-plane CH deform |
| | 1446 | 1459 | 30 | in-plane CH deform |
| | | 1298 | 2 | CC stretch |
| | | 1271 | 19 | CC stretch |
| | 1217 | 1227 | 42 | CF stretch |
| | | 1170 | 3 | in-plane CH deform |
| | 1137 | 1137 | 22 | in-plane CH deform |
| | 1101 | 1101 | 30 | in-plane CCC deform |
| | 1004 | 1032 | 3 | in-plane CCC deform |

| | | | |
|------------------|------|----|-------------------------|
| | 1025 | 1 | out-of-plane CH deform |
| | 974 | 3 | out-of-plane CH deform |
| | 876 | 1 | out-of-plane CH deform |
| 840 | 856 | 28 | in-plane CCC deform |
| 771 ^c | 769 | 70 | out-of-plane CH deform |
| | 741 | 7 | in-plane CCC deform |
| | 737 | 1 | out-of-plane CCC deform |

^a Calculated at the B3LYP/6-311++G(2d,2p) level with the anharmonic correction.

^b Overlapped with a band of atmospheric water.

^c Overlapped with a depletion band of *anti*-FBC.

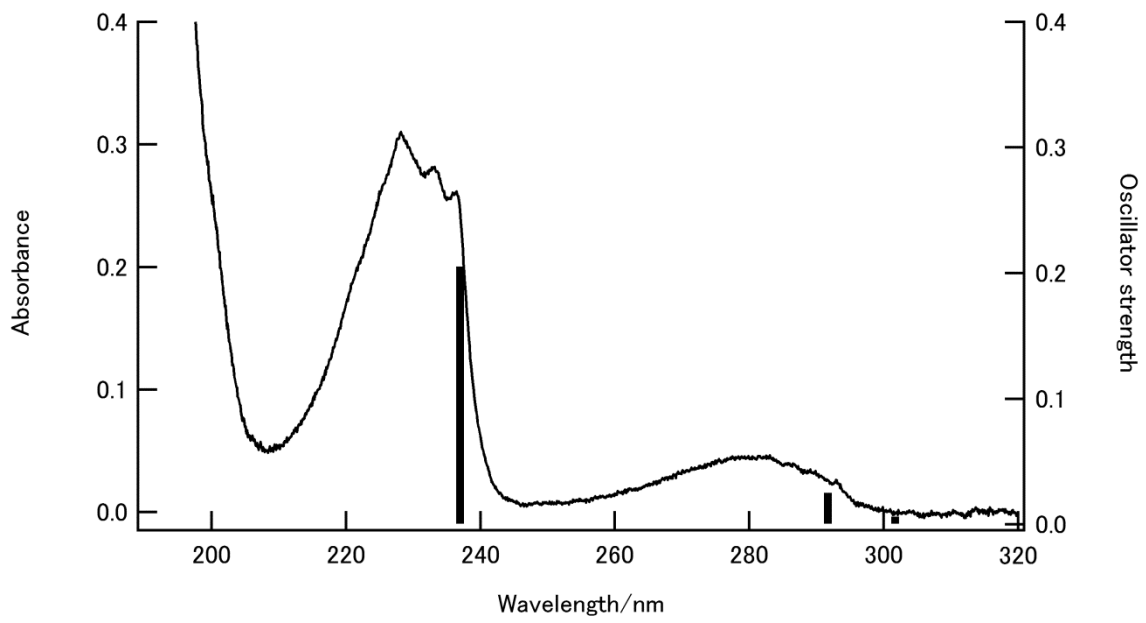


Fig. S1

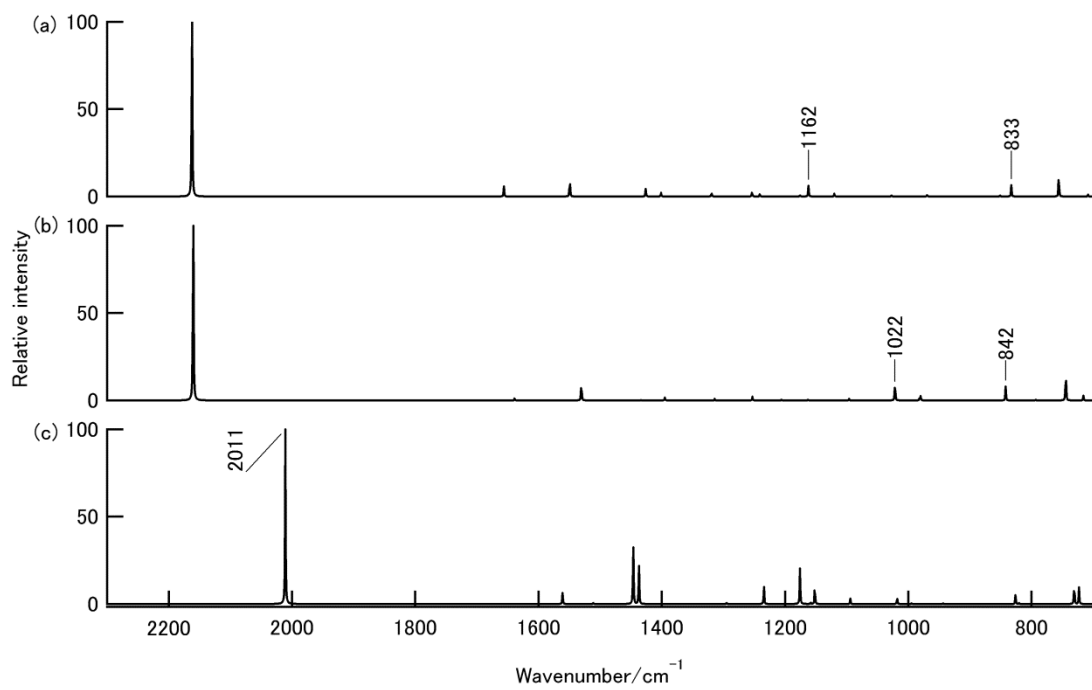


Fig. S2

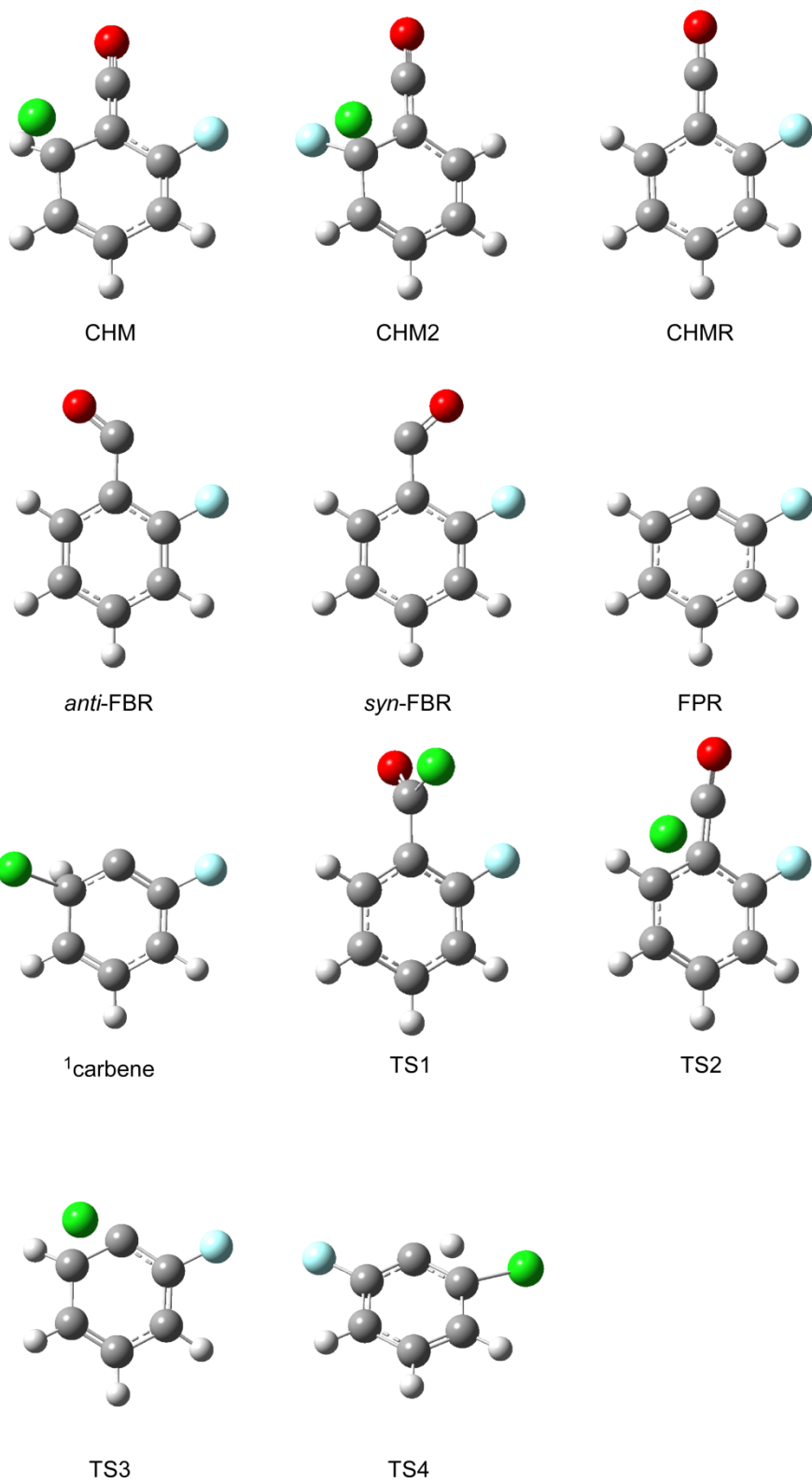


Fig. S3